Proc. Indian Acad. Sci. (*Chem. Sci.*), Vol. 115, No. 3, June 2003, pp 195–218

Chemical reactivity of the compressed noble gas atoms and their reactivity dynamics during collisions with protons

P K CHATTARAJ*, B MAITI and U SARKAR
Department of Chemistry, Indian Institute of Technology,
Kharagpur 721 302, India
e-mail: pkc@chem.iitkgp.ernet.in

MS received 18 December 2003; revised 25 April 2003

Abstract. Attempts are made to gain insights into the effect of confinement of noble gas atoms on their various reactivity indices. Systems become harder, less polarizable and difficult to excite as the compression increases. Ionization also causes similar effects. A quantum fluid density functional technique is adopted in order to study the dynamics of reactivity parameters during a collision between protons and He atoms in different electronic states for various projectile velocities and impact parameters. Dynamical variants of the principles of maximum hardness, minimum polarizability and maximum entropy are found to be operative.

Keywords. Confinement; reactivity dynamics; quantum fluid density functional theory.

1. Introduction

For some years now the influence of spatial confinement of atoms or molecules on their physical and chemical properties has been considered an important area of research. The concept of confined quantum systems[1] originated from the idea of simulating the effect of pressure on an atom by confining it in an impenetrable spherical box. This is useful for understanding the behaviour of: the effect of pressure on energy levels, polarizability of atoms and molecules,[1–19] semiconductor quantum dots, quantum wires, quantum wells etc.[20] Physical and chemical properties of systems are highly dependent on the size and shape of the confined volume.[20–30] In this article we have calculated the softness, polarizability, mean excitation energy, total energy and expectation values of r, r^2 and $1/r$ of He and Ne at various degrees of confinement.

Density functional theory[31] is successful in providing insights into the concepts of chemical reactivity parameters like hardness, polarizability, ionization energy etc. In DFT, the total energy functional for an N-electron system can be written as

$$E[\rho] = T[\rho] + E_x[\rho] + E_c[\rho] - \int \frac{Z}{r}\rho(\mathbf{r})\mathrm{d}\mathbf{r} + \frac{1}{2}\iint \frac{\rho(\mathbf{r})\rho(\mathbf{r}')}{|\mathbf{r}-\mathbf{r}'|}\mathrm{d}\mathbf{r}\mathrm{d}\mathbf{r}'. \quad (1)$$

We write

*For correspondence

$$T[\rho] = C_k \int \rho^{5/3}(\mathbf{r})\mathrm{d}\mathbf{r} - \frac{\lambda_1}{8}\int \frac{\mathbf{r}.\nabla\rho(\mathbf{r})}{\mathbf{r}^2}\mathrm{d}\mathbf{r},$$

is the kinetic energy functional;[32]

$$C_k = (3/10)(3\pi^2)^{2/3},$$

$$E_x = -C_x \int \rho^{4/3}(\mathbf{r})\mathrm{d}\mathbf{r},$$

$$\lambda_1 = 1/5,$$

is the Dirac local exchange energy functional;[33]

$$C_x = (3/4\pi)(3\pi^2)^{1/3},$$

$$E_c = -\int \frac{\rho(\mathbf{r})}{9\cdot 81 + 21\cdot 437\rho^{-1/3}}\mathrm{d}\mathbf{r},$$

is a Wigner type local correlation energy functional[34].

Electronegativity (χ)[35] and hardness (η)[36,37] which manifest the response of the system when N varies keeping while $v(\mathbf{r})$ is constant are respectively defined as

$$\chi = -\mu = -(\partial E/\partial N)_{v(\mathbf{r})}, \tag{2}$$

and

$$\eta = \tfrac{1}{2}(\partial^2 E/\partial N^2)_{v(\mathbf{r})} = \tfrac{1}{2}(\partial\mu/\partial N)_{v(\mathbf{r})}. \tag{3}$$

In (2) and (3) N, $v(\mathbf{r})$ and μ are the total number of electrons, external potential and chemical potential respectively. Electronegativity is the power of an atom in a molecule to attract electrons to itself.[38] Pearson[39] introduced the hardness concept through his hard–soft acid–base (HSAB) principle which states that 'hard likes hard and soft likes soft'. Apart from (3) hardness can also be defined as[40]

$$\eta = \frac{1}{N}\iint \eta(\mathbf{r},\mathbf{r}')f(\mathbf{r}')\rho(\mathbf{r})\mathrm{d}\mathbf{r}\mathrm{d}\mathbf{r}', \tag{4}$$

where $f(\mathbf{r})$ and $\eta(\mathbf{r}, \mathbf{r}')$ are the Fukui function[40,41] and hardness kernel[42] respectively. The Fukui function and hardness kernel are respectively defined as:

$$f(\mathbf{r}) = \left(\frac{\partial\rho(\mathbf{r})}{\partial N}\right)_{v(\mathbf{r})} = \left(\frac{\delta\mu}{\delta v(\mathbf{r})}\right)_N, \tag{5}$$

and

$$\eta(\mathbf{r},\mathbf{r}') = \frac{1}{2}\frac{\delta^2 F[\rho]}{\delta\rho(\mathbf{r})\delta\rho(\mathbf{r}')}, \tag{6}$$

where $F[\rho]$ is the Hohenberg–Kohn–Sham[43,44] universal functional of DFT.

Collisions of noble gas atoms with protons at low, intermediate and high-projectile velocities with different impact parameters have become an important area of research for theoreticians[45] and experimentalists[46] because such processes play an important role in nuclear physics and astrophysics. Theoretically, collision dynamics can be explained with the help of density functional theory (DFT)[31] by studying the ground- and excited-state electronic structure and properties of many-electron systems. According to DFT, the single-particle density $\rho(\mathbf{r})$ contains all the information about a system and the total energy attains a minimum value for the true $\rho(\mathbf{r})$. A time-dependent (TD) version of DFT is also available for an arbitrary TD potential whose mapping with the density has been shown to be uniquely invertible up to an additive TD function in the potential.[47] This TDDFT strengthens the quantum fluid dynamics (QFD).[48] For studying collision dynamics, we adopted a method, essentially an amalgamation of density functional theory (DFT) and quantum fluid dynamics (QFD), called the time-dependent quantum fluid density functional theory (TDQFDFT). Successful applications of TDQFDFT have already been made in intense laser-atom dynamics leading to photoionization[49] and photoemission,[50] suppression of ionization[51] and high energy H^+–Ne and H^+–He collisions.[52] We hope that these will lead to extensive applications of TDQFDFT to molecular dynamics, e.g. dissociation of molecules by an external field where the calculation of both nuclear and electronic motions ought to be considered. This adopts an impulse approximation, i.e., a straight-line trajectory for the projectile. In this article, we study the reactivity dynamics at different velocities and impact parameters. It is also important to know how the atom would response to the collision with a proton so far as its reactivity is concerned. The behaviour of the helium atom on collision with the proton can be explained with different reactivity parameters like electronegativity, hardness, polarizability, entropy, electrophilicity and nucleophilicity indices and uncertainty product. During the collision process, polarizability (α) is the corresponding response due to a change in $v(\mathbf{r})$ for constant N. A Shannon-type entropy (S) was introduced by Deb and Chattaraj[53] within a quantum fluid density functional framework. During molecule formation the electronegativity of the pertinent atoms get equalized.[54] A stable configuration or a favourable process is generally associated with maximum hardness (MH),[37] minimum polarizability (MP)[55] and maximum entropy (ME)[56] values. The conditions for maximum hardness and entropy as well as minimum polarizability complement the usual minimum energy criterion for stability. Recently Parr *et al*[57] have defined the electrophilicity index (W). We also study here the behaviour of ($1/W$), a valid candidate for the nucleophilicity index. It has also been shown recently[58] that the uncertainty product or the phase space volume (V_{ps}) is a measure of quantum fluctuations and hence has a bearing on the study of quantum domain behaviour of classically chaotic systems.

The theoretical background of the present work is provided in §2. Section 3 contains the numerical details, while results and discussions are given in §4. Finally, §5 presents some concluding remarks.

2. Theoretical background

The polarizability (α),[59,60] which is a measure of the response of the system by varying the external potential ($v(\mathbf{r})$) keeping the total number of electrons (N) constant, is calculated form the relation

$$\alpha = \left(\frac{4\pi}{3}\right)\int_0^\infty s(r)r^4 \mathrm{d}r. \tag{7}$$

The mean excitation energy[61] (I) in the local plasma approximation of charge distribution[62] is defined as follows:

$$I = 2\sqrt{\pi}\gamma \exp[-S_\rho / 2Z], \tag{8}$$

where S_ρ is the Shannon entropy and Z is the number of electrons of the atom. The chemical shift factor γ varies between 1 and $\sqrt{2}$.

The hardness kernel $\eta(\mathbf{r}, \mathbf{r}')$, (6), is calculated using the following local form for $F[\rho]$,

$$F[\rho] = T^{\text{local}}[\rho] + V_{ee}^{\text{local}}[\rho], \tag{9a}$$

where the local kinetic energy[63] and electron–electron repulsion energy[64] are taken as

$$T^{\text{local}}[\rho] = c_k \int \rho^{5/3}\mathrm{d}\mathbf{r} + c_x \int \frac{\rho^{4/3}/\mathbf{r}}{1+(r\rho^{1/3}/0{\cdot}043)}\mathrm{d}\mathbf{r}\,, \tag{9b}$$

and

$$V_{ee}^{\text{local}}[\rho] = 0{\cdot}7937(N-1)^{2/3}\int \rho^{4/3}\mathrm{d}\mathbf{r}. \tag{9c}$$

These local functionals are used because of the simplicity in the calculation of the second-order functional derivative and the associated Fukui function within this local model.

The dynamical polarizability is written as

$$\alpha(t) = | D_{ind}^z(t) | / | F_z(t) |, \tag{10a}$$

where $D_{ind}^z(t)$ is the electronic part of the induced dipole moment given as,

$$D_{ind}^z(t) = \int z\rho(\mathbf{r}, t)\mathrm{d}\mathbf{r}, \tag{10b}$$

and $F_z(t)$ is the z-component of the external Coulomb field due to the incoming proton.

The TD entropy is defined as,

$$S(t) = \int \left\{ \frac{5}{2} - \ln \rho(\mathbf{r}, t) + \frac{3}{2} \ln(k\theta(\mathbf{r}, t) / 2\pi) \right\} k\rho(\mathbf{r}, t) \mathrm{d}\mathbf{r}, \tag{11a}$$

where k is the Boltzmann constant and $\theta(\mathbf{r}, t)$ is a space–time dependent temperature given in terms of the kinetic energy density $t_s(\mathbf{r}, \rho(\mathbf{r}, t))$ as

$$t_s(\mathbf{r}; \rho(\mathbf{r}, t)) = \frac{3}{2} k\theta(\mathbf{r}, t)\rho(\mathbf{r}, t) + [|\, \mathbf{j}(\mathbf{r}, t)\,|^2 / 2\rho(\mathbf{r}, t)]. \tag{11b}$$

The electrophilicity index (W) is defined as

$$W = \mu^2 / 2\eta. \tag{12}$$

The term ($1/W$) is called the nucleophilicity index.

The phase space volume or the uncertainty product, V_{ps}[58,59] has been shown to be an important diagnostic of the quantum signature of classical chaos as related to the compactness of the electron cloud. For the present problem it may be defined as

$$\begin{aligned} V_{ps} = \{ &\langle (p_{\tilde{\rho}} - \langle p_{\tilde{\rho}} \rangle)^2 \rangle \langle (p_z - \langle p_z \rangle)^2 \rangle \\ &\langle (\tilde{\rho} - \langle \tilde{\rho} \rangle)^2 \rangle \langle (z - \langle z \rangle)^2 \rangle \}^{1/2}. \end{aligned} \tag{13}$$

A sharp increase in $V_{ps}(t)$ signals chaotic motion since it is a measure of the associated quantum fluctuations.

The dynamics of a quantum system are described in terms of the flow of a probability fluid associated with the probability density $\rho(\mathbf{r})$ and the current density $\mathbf{j}(\mathbf{r})$. The time evolution of these two quantities are governed by two basic QFD equations[53], viz. the equation of continuity,

$$(\partial\rho / \partial t) + \nabla \cdot (\rho \nabla \xi) = 0, \tag{14a}$$

and the equation of motion,

$$\frac{\partial \xi}{\partial t} + \frac{1}{2}(\nabla \xi)^2 + \frac{\delta G[\rho]}{\delta t} + \int \frac{\rho(\mathbf{r}, t)}{|\, \mathbf{r} - \mathbf{r}' \,|} \mathrm{d}\mathbf{r}' + v_{\mathrm{ext}}(\mathbf{r}, t) = 0, \tag{14b}$$

where ξ is the velocity potential. The universal functional $G[\rho]$ comprises kinetic and exchange correlation energy functionals and $v_{\mathrm{ext}}(\mathbf{r}, t)$ is the external potential. Atomic units are used throughout this article unless otherwise specified.

A three-dimensional complex-valued hydrodynamical function $\phi(\mathbf{r}, t)$ can be defined in the following polar form:

$$\phi(\mathbf{r}, t) = \rho(\mathbf{r}, t)^{1/2} \exp[i\xi(\mathbf{r}, t)], \tag{15a}$$

$$\rho(\mathbf{r}, t) = |\, \phi(\mathbf{r}, t)\,|^2, \tag{15b}$$

$$\mathbf{j}(\mathbf{r},t) = [\phi_{re}\nabla\phi_{im} - \phi_{im}\nabla\phi_{re}] = \rho\nabla\xi. \tag{15c}$$

A quantum fluid density functional theory (QFDFT)[53] was developed to study the time evolution of $\phi(\mathbf{r}, t)$ by combining (14) to generate the following generalized nonlinear Schrödinger equation (GNLSE) in cylindrical polar coordinates ($0 < \tilde{\rho} \leq \infty$; $-\infty \leq \tilde{z} \leq \infty$; $0 \leq \tilde{\phi} \leq 2\pi$),

$$\left[\frac{1}{2}\nabla^2_{\tilde{\rho},\tilde{z}} + V_{\text{eff}}(\rho; \tilde{\rho}, \tilde{z}, \tilde{\rho}_p, \tilde{z}_p, t)\right]\phi(\tilde{\rho}, \tilde{z}, \tilde{\rho}_p, \tilde{z}_p, t) = i\frac{\partial}{\partial t}\phi(\tilde{\rho}, \tilde{z}, \tilde{\rho}_p, \tilde{z}_p, t), \quad i = \sqrt{-1}, \tag{16}$$

$$V_{\text{eff}}(\rho; \tilde{\rho}, \tilde{z}, \tilde{\rho}_p, \tilde{z}_p, t) = \frac{\delta T_{NW}}{\delta\rho} + \frac{\delta E_{xc}}{\delta\rho} + \int\frac{\rho(\mathbf{r}', t)}{|\mathbf{r} - \mathbf{r}'|} + v_{\text{ext}}(\mathbf{r}, t), \tag{17}$$

where T_{NW} and E_{xc} denote the non-Weizsäcker part of the kinetic energy and exchange correlation energy functionals respectively. To construct the effective potential (17), of (16), we need T_{NW}, E_{xc} and $v_{\text{ext}}(\mathbf{r}, t)$. The explicit form for E_{xc} written as

$$E_{xc}[\rho] = E_x[\rho] + E_c[\rho], \tag{18a}$$

where E_x is a modified Dirac exchange functional:[63]

$$E_x[\rho] = -c_x\left[\int\rho^{4/3} + \int\frac{\rho^{4/3}\mathrm{d}\mathbf{r}}{1 + (\mathbf{r}^2\rho^{2/3}/0{\cdot}0244)}\mathrm{d}\mathbf{r}\right]; \tag{18b}$$

and $E_c[\rho]$ is a Wigner-type parametrized correlation energy functional given by

$$E_c[\rho] = -\int\frac{\rho}{9{\cdot}81 + 21{\cdot}437\rho^{-1/3}}\mathrm{d}\mathbf{r}. \tag{18c}$$

The kinetic energy functional for this problem is taken as

$$T[\rho] = c_k\int\rho^{5/3}\mathrm{d}\mathbf{r} + \frac{1}{8}\int\frac{\nabla\rho.\nabla\rho}{\rho}\mathrm{d}\mathbf{r} - a(N)\lambda\int\frac{\rho^{4/3}/\mathbf{r}}{1 + (\mathbf{r}\rho^{1/3}/0{\cdot}043)}\mathrm{d}\mathbf{r}, \tag{19a}$$

where

$$\lambda = 30(3/\pi)^{1/3}, \tag{19b}$$

$$a(N) = a_0 + a_1N^{-1/3} + a_2N^{-2/3}, \tag{19c}$$

$$a_0 = 0{\cdot}1279, \quad a_1 = 0{\cdot}1811, \quad a_2 = -0{\cdot}0819.$$

For studying the collision process between He atoms and protons the whole scattering system is considered a supermolecule and thus the corresponding kinetic energy functional comprises two parts:[58]

$$T[\rho] = T_{at}[\rho] + T_{mol}[\rho], \tag{20a}$$

where the atomic part $T_{at}[\rho]$ is taken as given in (18) and $T_{mol}[\rho]$ is given by

$$T_{mol}[\rho] = \iint \frac{1}{N^2}\left[\frac{1}{R^{12}} - \left(\frac{N}{10}\right)^{14} R^2 \exp(-0{\cdot}8R)\right] \rho(\mathbf{r})\rho(\mathbf{r}')\, \mathrm{d}\mathbf{r}\, \mathrm{d}\mathbf{r}', \tag{20b}$$

where R is the internuclear distance.

The form of $v_{ext}(\mathbf{r}, t)$ for the problem is taken as

$$v_{ext}(\mathbf{r}, t) = -\frac{2}{|R_1(t) - \mathbf{r}|} - \frac{1}{|R_2(t) - \mathbf{r}|'}, \tag{21}$$

where R_1 and R_2 are radius vectors of the target (He nucleus) and the projectile (H^+) respectively. The position of the target nucleus is chosen as the origin of the coordinate system and that of the projectile is determined by a classical trajectory.[65] The trajectory of the projectile is determined with the help of a classical equation of motion which is given by

$$M_P \frac{\mathrm{d}^2 R_2}{\mathrm{d}t^2} = -\nabla_{\mathbf{R}_2} \bigcup[E_P, \rho(\mathbf{R}_1, \mathbf{R}_2, t); Z_T Z_P, t] \tag{22a}$$

where

$$\mathbf{R}_1 = (\tilde{\rho}^2 + \tilde{z}^2)^{1/2}, \tag{22b}$$

and

$$\mathbf{R}_2 = (\tilde{\rho}_P^2(t) + \tilde{z}_P^2(t))^{1/2}. \tag{22c}$$

Here M_P is the mass of the projectile, E_P, its kinetic energy, Z_P and Z_T are nuclear charges of the projectile and target respectively. Relativistic contributions are not taken into account in this work. In the cylindrical coordinate system, (22a) can be written in compact matrix form as,

$$M_P \frac{\mathrm{d}^2}{\mathrm{d}t^2}\begin{pmatrix}\tilde{\rho}_P \\ \tilde{z}_P\end{pmatrix} = -\begin{pmatrix}\dfrac{\partial}{\partial\tilde{\rho}_P} & \dfrac{\partial}{\partial\tilde{\rho}_P} \\ \dfrac{\partial}{\partial\tilde{z}_P} & \dfrac{\partial}{\partial\tilde{z}_P}\end{pmatrix}\begin{pmatrix}\bigcup_1 \\ \bigcup_2\end{pmatrix}, \tag{23a}$$

where

$$\bigcup_1 = Z_P Z_T / (\tilde{\rho}_P + \tilde{z}_P)^{1/2}, \tag{23b}$$

and

$$\bigcup_2 = \int V_{\text{eff}}(\mathbf{r}_P, \mathbf{r}, t)\, \mathrm{d}\mathbf{r}. \tag{23c}$$

For the evolution of the first derivative with respect to $\tilde{z}_P$ and $\tilde{\rho}_P$ as well as the form of V_{eff} given by (17), (23a) can be simplified into two equations, viz.

$$M_P \frac{\mathrm{d}^2\tilde{\rho}_P}{\mathrm{d}t^2} = -\frac{Z_P Z_T \tilde{\rho}_P}{(\tilde{\rho}_P + \tilde{z}_P)^{3/2}} - Z_P \int \left[\int \rho(\tilde{\rho}, \tilde{z}, t) J_0(k\tilde{\rho}) J_1(k\tilde{\rho}_P) \exp(-k \mid \tilde{z} - \tilde{z}_P \mid) \mathrm{d}k \right] \mathrm{d}\mathbf{r} \tag{24}$$

and

$$M_P \frac{\mathrm{d}^2\tilde{z}_P}{\mathrm{d}t^2} = -\frac{Z_P Z_T \tilde{z}_P}{(\tilde{\rho}_P + \tilde{z}_P)^{3/2}} + Z_P \int \left[\int \rho(\tilde{\rho}, \tilde{z}, t) J_0(k\tilde{\rho}) J_0(k\tilde{\rho}_P) \exp(-k \mid \tilde{z} - \tilde{z}_P \mid) \{\pm k \mathrm{d}k\} \right] \mathrm{d}\mathbf{r}. \tag{25}$$

In (25), the '–' sign is taken if $\tilde{z} - \tilde{z}_P > 0$ and the '+' sign is taken if $\tilde{z} - \tilde{z}_P < 0$. In (24) and (25), J_0 and J_1 are the zeroth-order and first-order Bessel functions respectively. The finite-difference (central) forms of (24) and (25) can be written as

$$\tilde{\rho}_P^{n+1} = 2\tilde{\rho}_P^n - \tilde{\rho}_P^{n-1} + F_{\tilde{\rho}_P}^n (\mathrm{d}t)^2 / M_P, \tag{26}$$

and

$$\tilde{z}_P^{n+1} = 2\tilde{z}_P^n - \tilde{z}_P^{n-1} + F_{\tilde{z}_P}^n (\mathrm{d}t)^2 / M_P, \tag{27}$$

where the index n defines the discretized time domain. $F_{\tilde{\rho}_P}^n$ on the right-hand side of (25) is given by

$$F_{\tilde{\rho}_P}^n = -\frac{Z_P Z_T \tilde{\rho}_P^n}{\{(\tilde{\rho}_P^n)^2 + (\tilde{z}_P^n)^2\}^{3/2}} - Z_P \int \left[\int \rho(\tilde{\rho}, \tilde{z}, t) J_0(k\tilde{\rho}) k J_1(k\tilde{\rho}_P^n) \exp(-k \mid \tilde{z} - \tilde{z}_P^n \mid) \mathrm{d}k \right] 2\pi\tilde{\rho}\, \mathrm{d}\tilde{\rho}\, \mathrm{d}\tilde{z}, \tag{28}$$

while $F_{\tilde{z}_P}^n$ on the right-hand side of (26) is given by

$$F_{\tilde{\rho}_P}^n = -\frac{Z_P Z_T \tilde{z}_P^n}{\{(\tilde{\rho}_P^n)^2 + (\tilde{z}_P^n)^2\}^{3/2}} - Z_P \int \left[\int \rho(\tilde{\rho}, \tilde{z}, t) J_0(k\tilde{\rho}) k J_1(k\tilde{\rho}_P^n) \exp(-k \mid \tilde{z} - \tilde{z}_P^n \mid) \{\pm k \mathrm{d}k\} \right] 2\pi\tilde{\rho}\, \mathrm{d}\tilde{\rho}\, \mathrm{d}\tilde{z}. \tag{29}$$

Equations (26) and (27) indicate that in order to obtain the projectile's position $(\tilde{\rho}_P^{n+1}, \tilde{z}_P^{n+1})$ at any advanced $(n + 1)$th time step from the nth time step, one needs the

following quantities: (i) the electron density $\rho(\tilde{\rho}, \tilde{z}, \tilde{\rho}_P^n, \tilde{z}_P^n, t)$, (ii) the projectile's position at the nth time step $(\tilde{\rho}_P^n, \tilde{z}_P^n)$, and (iii) the projectile position at the $(n-1)$th time step $(\tilde{\rho}_P^{n-1}, \tilde{z}_P^{n-1})$.

The electron density of the colliding system for any position $(\tilde{\rho}_P^n, \tilde{z}_P^n)$ of the projectile can be calculated by solving (16). At any time, the projectile positions at *n*th and (*n*–1)th time steps can be obtained from the knowledge of the same at the first and second time steps. The projectile's position at the first time step ($t = 0$) is taken as

$$\tilde{z}_P^1 = -\tilde{z}_P^0; \quad \tilde{\rho}_P^1 = b, \tag{30a}$$

where b is the impact parameter. While that at the second time step ($t = \Delta t$) is taken as

$$\tilde{z}_P^2 = -\tilde{z}_P^1 + v_P \cos v_0 \Delta t, \tag{30b}$$

$$\tilde{\rho}_P^2 = -\tilde{\rho}_P^1 + v_P \sin v_0 \Delta t. \tag{30c}$$

Here v_P is the projectile's incident velocity and v_0 is the scattering angle.

$$v_P = (2E_P / M_P)^{1/2}. \tag{31}$$

Thus over a range of time the realistic path of the projectile at any incident energy can be calculated. The integrals appearing in (28) and (29) have been calculated by the trapezoidal method for the $\tilde{\rho}'$ and $\tilde{z}'$ variables, while a three-point Gauss quadrature has been employed for the variables *k*.

The validity of TDDFT allows us to legitimately assume that the mapping $v_{\text{ext}}(\mathbf{r}, t) \rightarrow \rho(\mathbf{r}, t)$ and $v_{\text{ext}}(\mathbf{r}, t) \rightarrow \mathbf{j}(\mathbf{r}, t)$ are uniquely invertible of $\rho(\mathbf{r}, t)$ and $\mathbf{j}(\mathbf{r}, t)$. Therefore in this context we can define a time-dependent energy quantity, $E(t)$ as a density functional as follows:

$$\begin{aligned} E(t) = \frac{1}{2}\int \rho(\mathbf{r}, t) |\nabla \xi|^2 \, d\mathbf{r} + T[\rho] + \frac{1}{2}\iint \frac{\rho(\mathbf{r}, t)\rho(\mathbf{r}', t)}{|\mathbf{r} - \mathbf{r}'|} d\mathbf{r}\, d\mathbf{r}' \\ + E_{xc}[\rho] + \int v_{\text{ext}}(\mathbf{r}, t)\rho(\mathbf{r}, t) d\mathbf{r}. \end{aligned} \tag{32}$$

A similar time-dependent energy functional was defined within a harmonic time-dependent perturbation by Deb and Ghosh[66] as well as by Bartolotti.[67] Runge and Gross[47] defined the same for a general time-dependent problem.

Now if there exists a point r_c where the sum of functional derivatives of total kinetic and exchange-correlation energies is equal to zero, the time-dependent chemical potential becomes equal to the total electrostatic potential at that point, that is:

$$-\chi(t) = \mu(t) = \int \frac{\rho(\mathbf{r}, t)}{|\mathbf{r}_c - \mathbf{r}|} d\mathbf{r} + v_{\text{ext}}(r_c, t), \tag{33a}$$

where r_c is the point at which the following condition is satisfied at that time step:

$$\frac{1}{2}(\nabla\xi)^2 + \frac{\delta T}{\delta\rho} + \frac{\delta E_{xc}}{\delta\rho} = 0. \tag{33b}$$

Since $j(\mathbf{r}, 0) = 0$, the above condition at $t = 0$ becomes identical to that of the ground state DFT given by Politzer *et al*[68] who showed through application of the electronegativity equalization principle that r_c values provide very good estimates of the covalent radii of the atom.

3. Computational details

Total energy is calculated from (1). The first term of (1) represents kinetic energy and the remaining terms represent potential energy. Numerical calculation of the self-consistent-field (SCF) electronic wavefunction has been done by using the standard Herman and Skillman[69] program. Since the wavefunction must vanish at the confining boundary, we have introduced this confinement condition by multiplying the un-normalized SCF wavefunction by a step function in each iteration. The step function taken here is given by[70]

$$\Theta = \exp[-(r/R)^{20}]. \tag{34}$$

The GNLSE was solved numerically using a leap-frog type of finite difference scheme. Azimuthal symmetry of the physical system allows us to analytically integrate over $0 \leq \tilde{\phi} \leq 2\pi$ in a cylindrical polar coordinate $(\tilde{\rho}, \tilde{\phi}, z)$ system. Equation (16) was transformed as

$$\left\{\left(\frac{3}{4x^3}\right)\frac{\partial y}{\partial x} - \left(\frac{1}{4x^2}\right)\frac{\partial^2 y}{\partial x^2} - \frac{\partial^2 y}{\partial z^2}\right\} - \left(\frac{1}{x^4} - 2v_{\text{eff}}\right)y = 2i\frac{\partial y}{\partial t}, \tag{35a}$$

where

$$y = \tilde{\rho}\phi, \tag{35b}$$

and

$$\tilde{\rho} = x^2. \tag{35c}$$

A detailed discussion on the numerical solution can be found elsewhere.[55] The numerical solution is launched with near-Hartree–Fock density of helium in the ^1S ground state[71] and a ^1P excited state[72] of the 1*s*2*p* electronic configuration. The temporal mesh size is taken as $\Delta t = 0{\cdot}025$ a.u. Different spatial grid sizes are chosen for the ground and excited states; we take $\Delta x = \Delta z = 0{\cdot}5$ a.u. and $\Delta x = \Delta z = 0{\cdot}036$ a.u. respectively. Large domains for x and z are taken when the excited-state density is used. Three different initial velocities of the projectile are $v_P = 0{\cdot}1$, $1{\cdot}0$ and $10{\cdot}0$. Two different values of b are also taken as $0{\cdot}6$ and $1{\cdot}2$. The values of scattering angle $(v_0) = 0{\cdot}0$. The value of M_P is 1836 a.u.

4. Results and discussions

Variation of softness with respect to cut-off radius R is shown in figure 1. A decrease of cut-off radius decreases the value of softness implies the fact that the system becomes

harder. The relative order of softness for He, He^+, Ne and Ne^+ is $S_{He^+} < S_{He} < S_{Ne^+} < S_{Ne}$, as expected. Atoms are softer than the corresponding ions.

Figure 2 presents the variation of polarizability (α) as a function of R. Polarizability is high for large values of R and decreases gradually as we decrease R. Polarizability or softness attains a saturation value for large values of R. The relative order of polarizability is same as softness. Polarizability decreases on ionization.

In figure 3 we present softness vs $\alpha^{1/3}$. It is clear from the figure that all curves are near-straight lines (regression coefficients are given in appropriate positions). For a confined system, the linear relation between S and $\alpha^{1/3}$ for He, He^+, Ne and Ne^+, as would have been expected[73–77] for atoms, molecules and clusters, is shown here for the first time.

Figure 4 depicts the plot of ionization energy (I) versus cut-off radius for He, He^+, Ne and Ne^+. From this figure it is clear that the increase of cut-off radius corresponds to a decrease in their mean excitation energy which is consistent with the expectation.[78] The I values for He and Ne are 35·390095 and 114·790594 respectively (for R = 10·0) which are very close to the values obtained by Hô *et al.*[62] Ions have higher I values than the corresponding atoms for all R values.

Figure 5 manifests how kinetic energy, potential energy and total energy change with radius. Kinetic energy increases more rapidly than potential energy with the decrease of cut-off radius. These plots are similar to those given by Gimarc[79] for He atom. The kinetic energy, potential energy and total energy values, given in table 1 which are very close to those obtained by Fischer[80] for free atoms (R = 10·0). For large I, virial theorem is satisfied in both the cases.

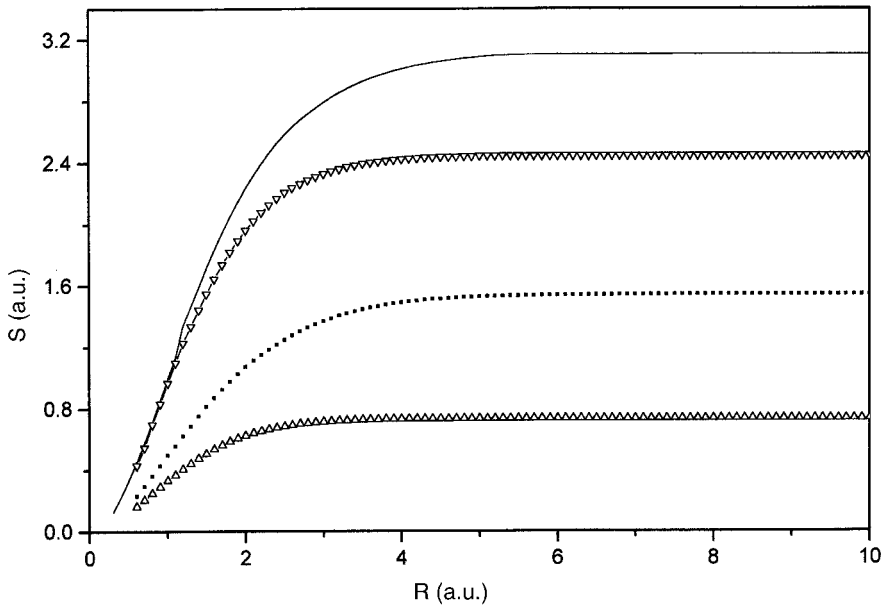

Figure 1. Plot of softness (S, a.u.) versus cut-off radius (R, a.u.) for He and Ne atoms and their ions confined in a spherical box. (·····) He atom, (—△—) He^+ ion, (——) Ne atom, (—▽—) Ne^+ ion.

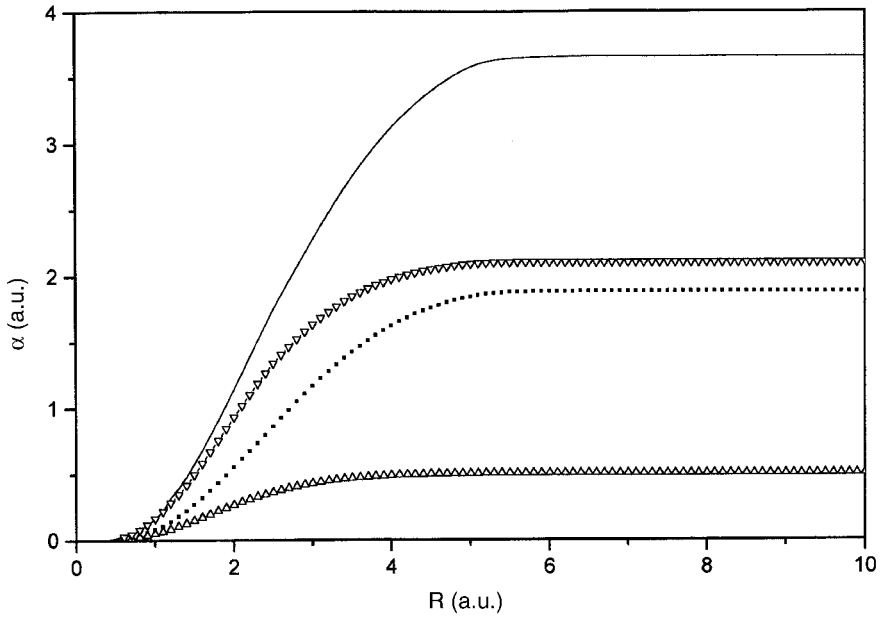

Figure 2. Plot of polarizability (α, a.u.) versus cut-off radius (R, a.u.) for He and Ne atoms and their ions confined in a spherical box. (·····) He atom, (—△—) He^+ ion, (——) Ne atom, (—▽—) Ne^+ ion.

Expectation values of r, r^2 and $1/r$ are listed in table 2 for total electronic charge density. Expectation values of these quantities for free (R = 10 a.u.) He atoms are in good agreement with those of Fischer.[81] Expectation values of r and r^2 decrease with decrease of R whereas expectation value of $1/r$ increases with decrease of R for both atoms and ions.

Evolution with time of different reactivity parameters is depicted in figures 6–12. All quantities are in atomic units. Unless otherwise specified, in all the figures, GS and ES refer to the ground and excited states of the helium atom respectively. Two different impact parameters and three different projectile velocities corresponding to b = 0·6, 1·2 and v_P = 0·1, 1·0, 10·0 are shown separately.

Figure 6 depicts the time-dependence of the chemical potential with different impact parameters (b) and different projectile velocities (v_P) in the collision process. Three distinct zones are discernible for the whole collision process: approach, encounter and departure. The concept of three collisional regimes was originally reported in terms of the time-dependent difference density and induced dipole moment profiles.[52] Since nowhere in space is condition (33b) satisfied in the encounter regime, neither r_c nor μ is calculable. After the initial transients leave, μ becomes more or less stable at the approach regime. Towards the end of the approach regime and the beginning of the departure regime μ changes drastically due to the rapid charge oscillations. These time steps bracket the encounter regime where the electron density is shared by both nuclei. While μ in these time steps is mainly negative for the ground state, it becomes both positive and negative

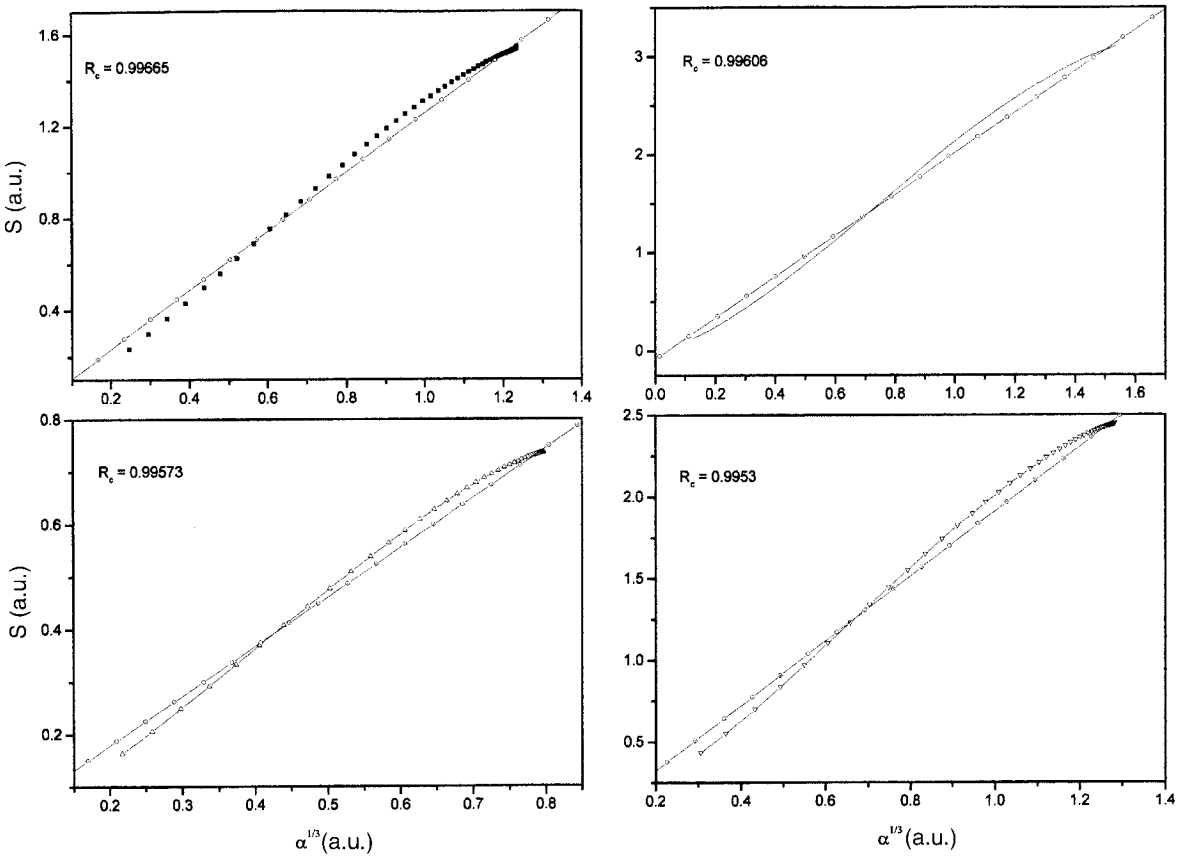

Figure 3. Plot of softness (S, a.u.) versus $\alpha^{1/3}$ (a.u.) for He and Ne atoms and their ions confined in a spherical box. (·····) He atom, (—△—) He^+ ion, (——) Ne atom, (—▽—) Ne^+ ion and (—⊙—) best fit line.

Table 1. Variation of potential, kinetic and total energies (in a.u.) versus the cut-off radius (R, a.u.) for He and Ne atoms and theirs ions.

Atom/ion	R	Potential energy	Kinetic energy	Total energy
He	10·0	–5·5854	2·6794	–2·9060
	8·0	–5·5854	2·6794	–2·9060
	6·0	–5·5854	2·6794	–2·9060
	4·0	–5·5880	2·6827	–2·9052
	3·0	–5·6067	2·7077	–2·8990
	2·0	–5·7531	2·9062	–2·8470
	1·5	–6·0843	3·4048	–2·6795
	1·0	–7·1464	5·1804	–1·9660
	0·8	–8·1288	7·2270	–0·9018
	0·6	–9·9263	11·8669	1·9407
	0·4	–14·4348	25·7071	11·2723
	0·3	–18·3581	44·5086	26·1504
He^+	10·0	–3·8010	1·2274	–2·5736
	8·0	–3·8010	1·2274	–2·5736
	6·0	–3·8010	1·2274	–2·5736
	4·0	–3·8011	1·2275	–2·5736
	3·0	–3·8045	1·2298	–2·5747
	2·0	–3·8603	1·2701	–2·5902
	1·5	–4·0332	1·4062	–2·6270
	1·0	–4·6412	1·9574	–2·6838
	0·8	–5·2376	2·6118	–2·6258
	0·6	–6·3462	4·0975	–2·2487
	0·4	–8·6796	8·2178	–0·4618
	0·3	–11·1066	14·1795	3·0729
Ne	10·0	–258·1772	128·2573	–129·9199
	8·0	–258·1771	128·2572	–129·9199
	6·0	–258·1747	128·2544	–129·9203
	4·0	–258·1778	128·2630	–129·9148
	3·0	–258·2279	128·3548	–129·8731
	2·0	–258·7100	129·2800	–129·4300
	1·5	–260·4154	132·5628	–127·8526
	1·0	–277·8467	158·6617	–119·1850
	0·8	–292·3612	185·9834	–106·3778
	0·6	–324·3163	246·9639	–77·3524
	0·4	–434·1629	489·6910	55·5281
	0·3	–554·4364	845·8103	291·3738
Ne^+	10·0	–256·5539	126·0408	–130·5131
	8·0	–256·5539	126·0408	–130·5131
	6·0	–256·5538	126·0407	–130·5131
	4·0	–256·5560	126·0433	–130·5127
	3·0	–256·5974	126·0911	–130·5063
	2·0	–257·0275	126·6993	–130·3282
	1·5	–258·7490	129·2318	–129·5172
	1·0	–266·3955	141·6721	–124·7234
	0·8	–277·6087	161·7620	–115·8466
	0·6	–316·3342	222·0182	–94·3160
	0·4	–425·5261	438·8206	13·2945
	0·3	–544·1743	757·7473	213·5730

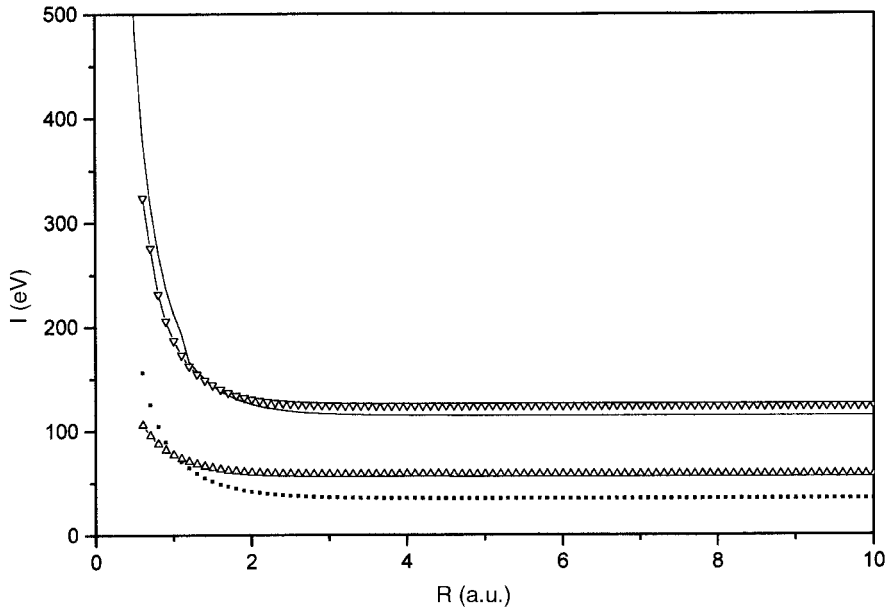

Figure 4. Plot of mean excitation energy (I, eV) versus cut- off radius (R, a.u.) for He and Ne atoms and their ions confined in a spherical box. (·····) He atom, (—△—) He^+ ion, (——) Ne atom, (—▽—) Ne^+ ion.

in excited state. In the departure regime, μ again changes drastically to reach a stable value more or less the same as at obtained in the approach regime.

The departure regime starts at $t = 10{\cdot}975$ a.u. onward, where we see again strong oscillations, indicating the charge readjustment and the return of electron density to the helium atom leaving the proton. Even after the proton moves a considerable distance away, the helium atom keeps on pulsating for quite some time. In the excited state, similar features are noticed.

Time evolution of the hardness is shown in figure 7. Hardness attains a maximum value in the encounter regime which may be considered to be a dynamical variant of the maximum hardness principle (MHP). The η_{max} values are shown in the table 3 with different projectile velocities, different impact parameters and different states. The η_{max} values for the ground state are greater than excited state and it increases with an increase in the projectile velocities and impact parameters, as expected from the MHP. It may be noted that here η is calculated as a density functional and it does not require the ionization potential, electron affinity or orbital energy values per se. In the approach regime, η remains more or less static. It suddenly increases and passes through a maximum in the encounter regime. The maximization of η in the encounter regime and the larger η_{max} value for the ground state clearly reflect the validity of the maximum hardness principle in a dynamical context. In the departure regime, η attains the same steady value as in the approach regime. With increasing the projectile velocity and impact parameter the value of the η increases.

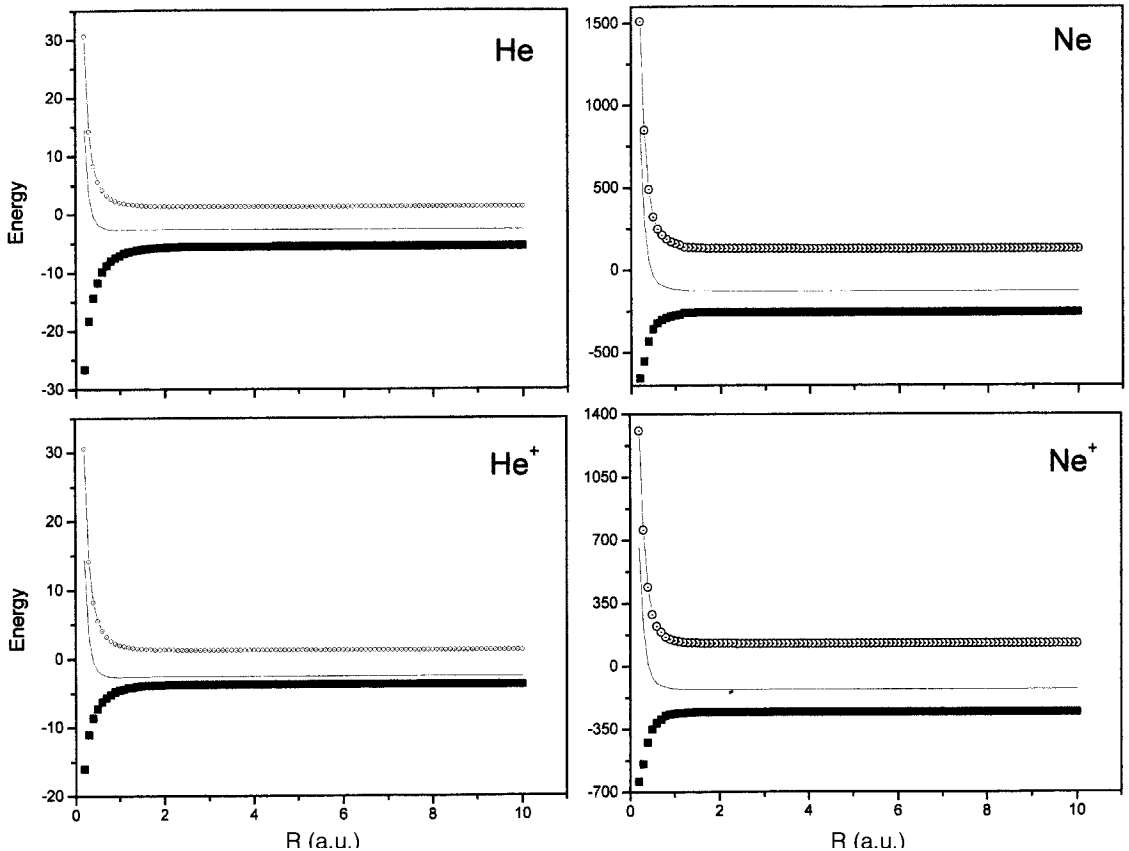

Figure 5. Plot of mean kinetic energy, potential energy, total energy (a.u.) versus cut-off radius (R, a.u.) for He and Ne atoms and their ions confined in a spherical box. (·····) potential energy, (—⊙—) kinetic energy and (——) total energy.

Table 2. Expectation values (in a.u.) of $\langle r \rangle$, $\langle r^2 \rangle$ and $\langle 1/r \rangle$ for different cut-off radii (R, a.u.) for He and Ne atoms and their ions.

Atom/ion	R	$\langle r \rangle$	$\langle r^2 \rangle$	$\langle 1/r \rangle$
He	10·0	0·940246	1·233518	1·692418
	8·0	0·940246	1·233514	1·692418
	6·0	0·940149	1·232840	1·692441
	4·0	0·936164	1·211827	1·693617
	3·0	0·917871	1·135408	1·701663
	2·0	0·842262	0·898776	1·756841
	1·5	0·744267	0·669505	1·876700
	1·0	0·581541	0·388410	2·224868
	0·8	0·490569	0·271528	2·554247
	0·6	0·383892	0·163573	3·162193
	0·4	0·261344	0·075227	4·572030
	0·3	0·200234	0·043870	5·884057
He^+	10·0	0·750006	0·750049	2·000165
	8·0	0·750006	0·750049	2·000165
	6·0	0·750005	0·750045	2·000165
	4·0	0·749831	0·749259	2·000266
	3·0	0·747358	0·740224	2·002134
	2·0	0·720049	0·664792	2·032839
	1·5	0·662078	0·539825	2·127145
	1·0	0·538638	0·339324	2·450310
	0·8	0·461439	0·244000	2·770124
	0·6	0·366936	0·151201	3·365776
	0·4	0·260622	0·074860	4·588757
	0·3	0·199988	0·043775	5·893574
Ne	10·0	0·766285	0·894939	3·171599
	8·0	0·766285	0·894937	3·171599
	6·0	0·766226	0·894497	3·171607
	4·0	0·764159	0·882862	3·172010
	3·0	0·755831	0·845805	3·174471
	2·0	0·719130	0·723767	3·192610
	1·5	0·664639	0·586512	3·240234
	1·0	0·514937	0·332243	3·565481
	0·8	0·442907	0·239045	3·831170
	0·6	0·359049	0·152396	4·324632
	0·4	0·246313	0·071268	5·948437
	0·3	0·180601	0·038165	7·731242
Ne^+	10·0	0·693915	0·716706	3·424285
	8·0	0·693915	0·716706	3·424285
	6·0	0·693912	0·716688	3·424285
	4·0	0·693576	0·714941	3·424372
	3·0	0·690648	0·702866	3·425612
	2·0	0·668234	0·632051	3·438727
	1·5	0·625324	0·527982	3·481505
	1·0	0·527875	0·351825	3·645816
	0·8	0·458432	0·257318	3·866957
	0·6	0·354716	0·150316	4·490940
	0·4	0·241923	0·069564	6·186403
	0·3	0·176244	0·036761	8·045274

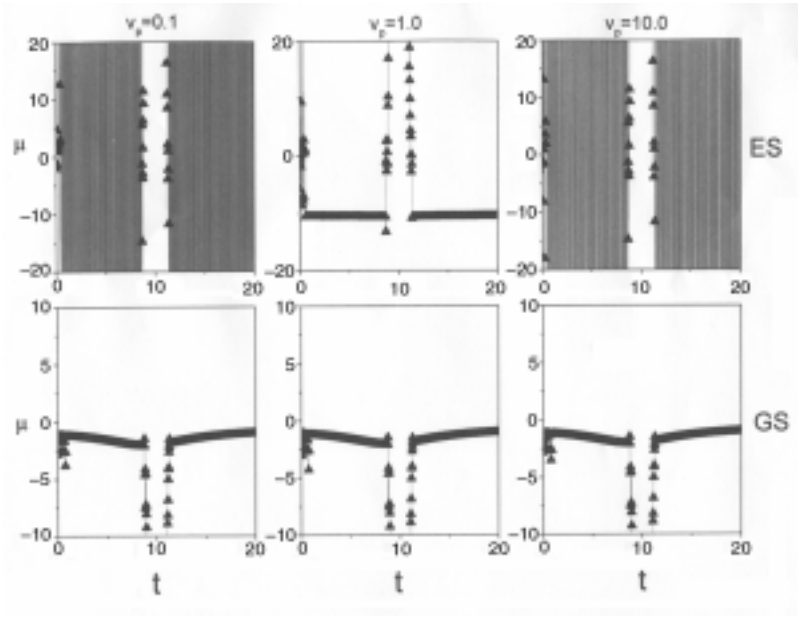

Figure 6. Time (a.u.) evolution of chemical potential (μ, a.u.) during a collision process between a He atom and a proton (*GS*, ground state; *ES*, excited state): v_p = 0·1, 1·0, 10·0; (—) b = 0·6, (▲▲▲) b = 1·2.

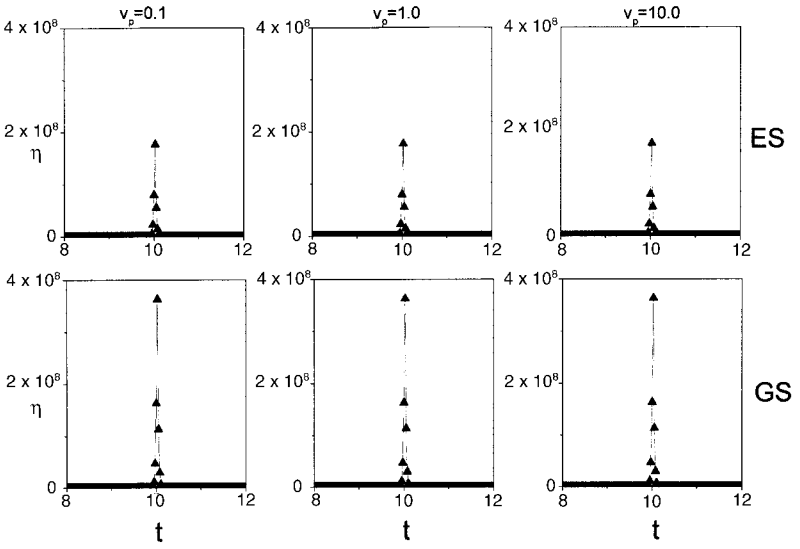

Figure 7. Time (a.u.) evolution of hardness (η, a.u.) during a collision process between a He atom and a proton (*GS*, ground state; *ES*, excited state): v_p = 0·1, 1·0, 10·0; (—) b = 0.6, (▲▲▲) b = 1·2.

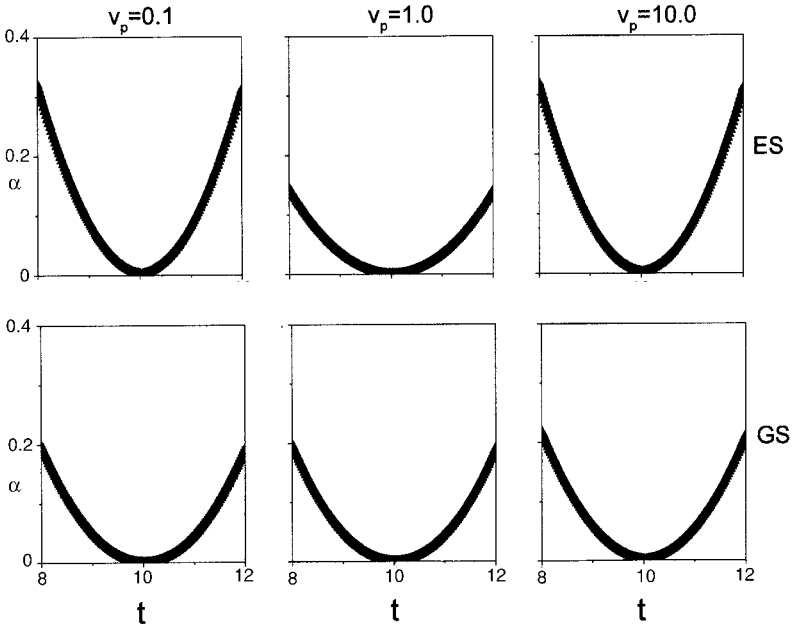

Figure 8. Time (a.u.) evolution of polarizability (α, a.u.) during a collision process between a He atom and a proton (*GS*, ground state; *ES*, excited state): v_p = 0·1, 1·0, 10·0; (—) b = 0·6, (▲▲▲) b = 1·2.

Table 3. The η_{max}, α_{min}, S_{max} and V_{ps} values at the closest approach during the collision between He atoms in the ground and excited states and protons (v_p = 0·1, 1·0, 10·0; b = 0·6, 1·2). All units are atomic units.

	b = 0·6		b = 1·2	
	GS	*ES*	*GS*	*ES*
v_p = 0·1				
η_{max}	$3{\cdot}62700 \times 10^{8}$	$1{\cdot}76870 \times 10^{8}$	$3{\cdot}62730 \times 10^{8}$	$1{\cdot}76873 \times 10^{8}$
α_{min}	$7{\cdot}58761 \times 10^{-5}$	$2{\cdot}77000 \times 10^{-4}$	$7{\cdot}58751 \times 10^{-5}$	$2{\cdot}66700 \times 10^{-4}$
S_{max}	57·87625	48·05389	57·87627	48·05689
V_{ps}	10·11640	36·67314	10·22740	36·82273
v_p = 1·0				
η_{max}	$3{\cdot}62700 \times 10^{8}$	$1{\cdot}76872 \times 10^{8}$	$3{\cdot}62750 \times 10^{8}$	$1{\cdot}76875 \times 10^{8}$
α_{min}	$7{\cdot}58447 \times 10^{-5}$	$2{\cdot}54218 \times 10^{-4}$	$7{\cdot}58441 \times 10^{-5}$	$2{\cdot}54217 \times 10^{-4}$
S_{max}	57·87780	49·62760	57·87790	49·62800
V_{ps}	10·13710	6175·56150	10·23710	6818·17770
v_p = 10·0				
η_{max}	$3{\cdot}62740 \times 10^{8}$	$1{\cdot}76875 \times 10^{8}$	$3{\cdot}62770 \times 10^{8}$	$1{\cdot}76877 \times 10^{8}$
α_{min}	$1{\cdot}15000 \times 10^{-5}$	$2{\cdot}07000 \times 10^{-4}$	$1{\cdot}05000 \times 10^{-5}$	$2{\cdot}17000 \times 10^{-4}$
S_{max}	57·87928	49·72670	57·895280	49·82270
V_{ps}	10·13910	19204·10200	10·38110	19870·74000

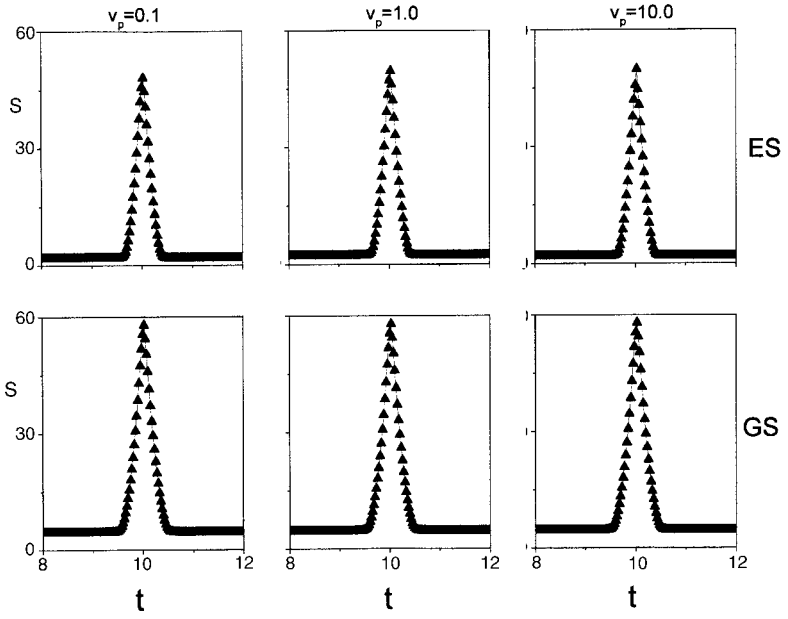

Figure 9. Time (a.u.) evolution of entropy (*S*, a.u.) during a collision process between a He atom and proton (*GS*, ground state; *ES*, excited state): v_p = 0·1, 1·0, 10·0; (—) b = 0·6, (▲▲▲) b = 1·2.

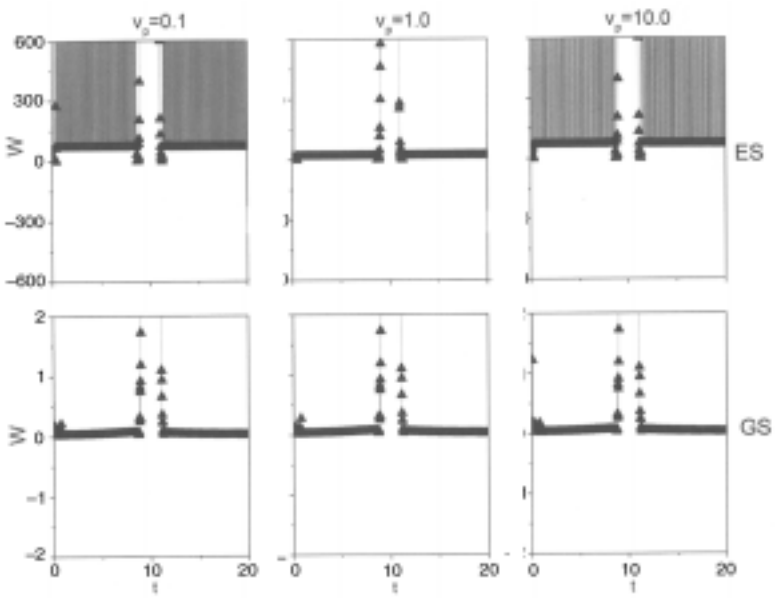

Figure 10. Time (a.u.) evolution of electrophilicity index (*W*, a.u.) during a collision process between a He atom and proton (*GS*, ground state; *ES*, excited state): v_p = 0·1, 1·0, 10·0; (—) b = 0.6, (▲▲▲) b = 1·2.

Figure 8 presents the time evolution of the dynamical polarizability. We notice that α becomes minimum in the encounter regime and a smaller α value for the ground state than for the excited state which is in conformity with the minimum polarizability principle (MPP). The α_{min} values for the ground and excited states are shown in the table 3 with different projectile velocities and different impact parameters. It may be noted that the α_{min} values of the ground state are less than those of the excited state with an increase in the projectile velocity and the impact parameter as expected from the MPP. Once the initial transients die out, α gradually decreases and passes through a minimum in the encounter regime when the two nuclei come closest to each other, as expected. The α_{min} values decrease as b and v_p increase.

Figure 9 presents the time-dependent entropy. Once the initial undulations disappear, *S* attains a steady value at the approach regime. In the encounter regime, it suddenly increases and passes through a maximum. In the departure regime *S* attains the same steady value as in the approach regime. The maximum entropy principle reveals itself in these findings. The S_{max} values for the ground state and excited state are given in table 3 for different projectile velocities, different impact parameters and different states. The value of S_{max} increases with increasing projectile velocity and impact parameter in both ground and excited states. The values of *S* in the ground state are greater than those of excited state.

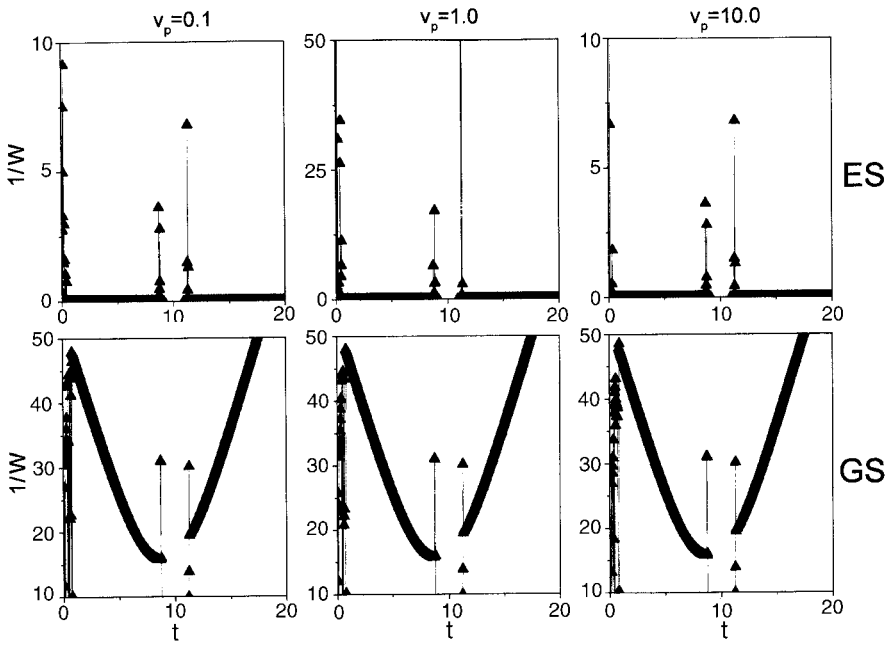

Figure 11. Time (a.u.) evolution of nucleophilicity index (1/*W*, a.u.) during a collision process between a He atom and proton (*GS*, ground state; *ES*, excited state): v_p = 0·1, 1·0, 10·0; (—) *b* = 0·6, (▲▲▲) *b* = 1·2.

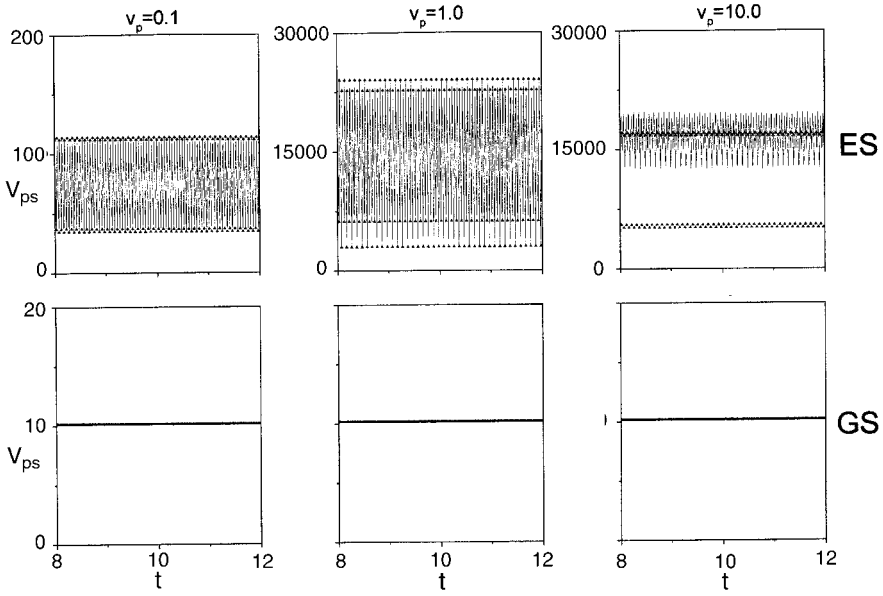

Figure 12. Time (a.u.) evolution of phase volume (V_{ps}, a.u.) during a collision process between a He atom and proton (*GS*, ground state; *ES*, excited state): v_p = 0·1, 1·0, 10·0; (—) b = 0.6, (▲▲▲) b = 1·2.

Figure 10 presents the dynamic profile of electrophilicity index (W). The plots look like the plots of chemical potential (μ) for different projectile velocities and impact parameters in both ground and excited states.

Figure 11 presents the dynamic profile of nucleophilicty index ($1/W$). These plots are much simpler than the plots of chemical potential (μ)/electrophilicity index (W).

Figure 12 shows the phase volume or the uncertainty product, V_{ps}. It confirms that the quantum fluctuations are always larger in the excited state than in the ground state as is expected from the more compactness of the ground state electron cloud. The values of V_{ps} at the closest approach are listed in table 3 for different velocities, impact parameters and electronic states. V_{ps} values increase with those of b and v_p. A small portion of this work is published elsewhere.[81]

4. Concluding remarks

Various reactivity indices like softness, polarizability and mean excitation energy are studied for confined He and Ne atoms and their ions. This method shows that when the radius of the confining box increases, softness, polarizability and $\langle 1/r \rangle$ increase but ionization energy (I), total energy (E), $\langle r \rangle$ and $\langle r^2 \rangle$ decrease. Increasing value of I mimics the fact that more energy is needed for excitation which is also supported by the decreasing nature of the softness and polarizability. As expected, He^+ and Ne^+ are harder and less polarizable with larger excitation energies compared to their neutral atom counterparts. Therefore this method provides new physical insights into the problem of reactivity indices as well as total energy of the compressed systems.

On the other hand, a quantum fluid density functional approach is found to be adequate in understanding the dynamics of ground- and excited-state electron densities of a helium atom interacting with an incoming proton. Dynamics of various reactivity parameters like electronegativity, hardness, polarizability, entropy, electrophilicity and nueleophilicity indices and phase space volume are studied. The whole collision process can be divided into approach, encounter and departure regimes in terms of the time-dependent chemical potential profile. In the encounter regime where the actual chemical process takes place, hardness and entropy maximize and polarizability minimizes. Dynamical variants of the maximum hardness principle, maximum entropy principle and minimum polarizability principle are observed to be valid for both electronic states and different values of impact parameters and projectile velocities.

Acknowledgements

We thank Prof. S S Krishnamurthy for kindly inviting us to publish the paper in this journal, the Council of Scientific and Industrial Research, New Delhi for financial support and the referee for constructive criticism.

References

1. Michels A, de Boer J and Bijl A 1937 *Physica* **4** 981
2. Sommerfeld A and Welker H 1928 *Ann. Phys.* **32** 56
3. de Groot S R and ten Seldam C A 1946 *Physica* **12** 669
4. ten Seldam C A and de Groot S R 1952 *Physica* **18** 891
5. Cottrell T L 1951 *Trans. Faraday Soc.* **47** 37
6. Gimarc B M 1966 *J. Chem. Phys.* **44** 373
7. Suryanarayana D and Weil J A 1976 *J. Chem. Phys.* **64** 510
8. Ley-Koo E and Rubinstein S 1979 *J. Chem. Phys.* **71** 351
9. Fernandez F M and Castro E A 1982 *Int. J. Quantum Chem.* **21** 741
10. Arteca G A, Fernandez F M and Castro E A 1984 *J. Chem. Phys.* **80** 1569
11. Fröman P O, Yngve S and Fröman N 1987 *J. Math. Phys.* **82** 1813
12. Yngve S J 1988 *J. Math. Phys*. **29** 931
13. Gorecki J and Byers B W 1987 *J. Phys.* **B20** 5953
14. Goodfriend P L 1990 *J. Phys.* **B23** 1373
15. Marin J L and Cruz S A 1991 *J. Phys.* **B24** 2899
16. Marin J L and Cruz S A 1991 *Am. J. Phys*. **59** 931
17. Goldman S and Joslin C 1992 *J. Phys. Chem*. **96** 6021
18. Brownstein K R 1993 *Phys. Rev. Lett*. **71** 1427
19. Dutt R, Mukherjee A and Varshni Y P 1995 *Phys. Rev. A*. **52** 1750
20. Jaskólski W 1996 *Phys. Rep.* **271** 1, and references therein
21. Ley-Koo E and Flores-Flores A 1998 *Int. J. Quantum Chem.* **66** 123
22. Ludeña E V 1978 *J. Chem. Phys.* **69** 1770
23. Ludeña E V and Gregori M 1979 *J. Chem. Phys.* **71** 2235
24. Gorecki J and Byers Brown W 1988 *J. Phys.* **B21** 403
25. LeSar R and Herschbach D R 1981 *J. Phys. Chem*. **85** 2804
26. LeSar R and Herschbach D R 1983 *J. Phys. Chem*. **87** 5202
27. Marin J L and Cruz S A 1992 *J. Phys.* **B25** 4365
28. Marin J L and Cruz S A 1995 *J. Mol. Struct.* (*Theochem*.) **287** 281
29. Marin J L, Rosas R and Uribe A 1995 *Am. J. Phys.* **63** 460
30. Corella-Madueño A, Rosas R, Marin J L and Riera R 1999 *Phys. Low Dim. Struct.* **5/6** 75
31. Parr R G and Yang W 1989 *Density functional theory of atoms and molecules* (New York Oxford University Press)
32. Haq S, Chattaraj P K and Deb B M 1984 *Chem. Phys. Lett.* **111** 79
33. Dirac P A M 1930 *Proc. Cambridge Phil. Soc.* **26** 376

34. Brual G and Rothstein S M 1978 *J. Chem. Phys.* **69** 1177
35. Sen K D and Jorgensen C K (eds) 1987 *Electronegativity, structure and bonding* (Berlin: Springer-Verlag) vol 66
36. Pearson R G 1997 *Chemical hardness: Application form molecules to solids* (Weinheim: Wiley-VCH Verlag)
37. Sen K D (eds) 1993 *Chemical hardness: Structure and bonding* (Berlin: Springer-Verlag) vol 80
38. Pauling L 1960 *The Nature of the chemical bond* 3rd edn (Ithaca: Cornell University Press)
39. Pearson R G 1990 *Coord. Chem. Rev.* **100** 403
40. Pearson R G 1973 *Hard and soft acids and bases* (Stroudsberg, PA: Dowden, Hutchinson & Ross)
41. Fukui K 1982 *Science* **218** 747
42. Berkowitz M, Ghosh S K and Parr R G 1999 *J. Am. Chem. Soc.* **121** 1922
43. Hohenberg P and Kohn W 1964 *Phys. Rev.* **B136** 864
44. Kohn W and Sham L G 1965 *Phys. Rev.* **A140** 1133
45. Kulander K C, Sandhya Devi K R and Koonin S E 1982 *Phys. Rev.* **A25** 2968
46. Rudd M E, Kim Y K, Madison D H and Gay T J 1992 *Rev. Mod. Phys.* **64** 441
47. Runge E and Gross E K U 1984 *Phys. Rev. Lett.* **52** 997
48. Madelung E 1926 *Z. Phys.* **40** 322
49. Dey B K and Deb B M 1995 *Int. J. Quant. Chem.* **56** 707
50. Dey B K and Deb B M 1998 *Int. J. Quant. Chem.* **70** 441
51. Dey B K and Deb B M 1997 *Pramana J. Phys.* **48** L849
52. Deb B M, Chattaraj P K and Mishra S 1991 *Phys. Rev.* **A43** 1248
53. Deb B M and Chattaraj P K 1989 *Phys. Rev.* **A39** 1696
54. Sanderson R T 1951 *Science* **114** 670
55. Chattaraj P K and Sengupta S 1996 *J. Phys. Chem.* **100** 16126
56. Jaynes E T 1963 In *Statistical physics* (ed.) K W Ford, Brandeis Lectures (New York: Benjamin) vol 3
57. Parr R G, Szentpaly L V and Liu S 1999 *J. Am. Chem. Soc.* **121** 1922
58. Chattaraj P K and Sengupta S 1999 *J. Phys. Chem.* **A103** 6122
59. Fuentealba P 1995 *J. Chem. Phys.* **103** 6571
60. Garza J and Robles J 1993 *Phys. Rev.* **A47** 2680
61. Ahlen S P 1980 *Rev. Mod. Phys.* **52** 121
62. Hồ M, Weaver D F Jr and Smith V H 1998 *Phys. Rev.* **A57** 4512
63. Ghosh S K and Deb B M 1994 *J. Phys.* **B27** 381
64. Parr R G 1988 *J. Phys. Chem.* **92** 3060
65. Dey B K and Deb B M 1998 *Int. J. Quantum Chem.* **67** 251
66. Deb B M and Ghosh S K 1982 *J. Chem. Phys.* **77** 342
67. Bartolotti L J 1981 *Phys. Rev.* **A24** 1661
68. Politzer R P, Parr R G and Murphy D R 1983 *J. Chem. Phys.* **79** 3859
69. Herman F and Skillman S 1963 *Atomic structure calculations* (Englewood Cliffs, NJ: Prentice Hall)
70. Boeyens J C A 1994 *J. Chem. Soc., Faraday Trans.* **90** 3377
71. Clementi E and Roetti C 1974 *At. Data Nucl. Data Tab.* **14** 174
72. Mukherjee P K, Sengupta S and Mukherji A 1970 *Int. J. Quant. Chem.* **4** 139
73. Politzer P 1987 *J. Chem. Phys.* **86** 1072
74. Ghanty T K and Ghosh S K 1993 *J. Phys. Chem.* **97** 4951
75. Hati S and Datta D 1994 *J. Phys. Chem.* **98** 10451
76. Fuentealba P and Reyes O 1993 *J. Mol. Struct.* (*Theochem.*) **282** 65
77. Roy R K, Chandra A K and Pal S 1995 *J. Mol. Struct.* (*Theochem.*) **331** 261
78. Sabin P B and Sabin J R 2001 *Int. J. Quantum Chem.* **82** 277
79. Gimarc B M 1967 *J. Chem. Phys.* **47** 5110
80. Fischer C F 1977 *The Hartree–Fock method for atoms: A numerical approach* (New York: Wiley-Interscience)
81. Chattaraj P K and Sarkar U 2003 *Chem. Phys. Lett.* **372** 805